

# Serine Proteases: An Ab initio Molecular Dynamics Study

L. De Santis<sup>(1,2)</sup> and P. Carloni<sup>(1,2,3)</sup>

<sup>1</sup> INFN – Istituto Nazionale di Fisica della Materia

<sup>2</sup> ISAS – International School for Advanced Studies,

Via Beirut 4, 34014 Trieste, Italy

<sup>3</sup> International Center for Genetic Engineering and Biotechnology,

AREA Science Park, Padriciano 99, 34012, Trieste, Italy

**ABSTRACT.** In serine proteases (SP's), the H-bond between His-57 and Asp-102, and that between Gly-193 and the transition state intermediate play a crucial role for enzymatic function. To shed light on the nature of these interactions, we have carried out ab initio molecular dynamics simulations on complexes representing adducts between the reaction intermediate and elastase (one protein belonging to the SP family). Our calculations indicate the presence of a low-barrier H-bond between His-57 and Asp-102, in complete agreement with NMR experiments on enzyme-transition state analog complexes [1]. Comparison with an ab initio molecular dynamics simulation on a model of the substrate-enzyme adduct indicates that the Gly-193-induced strong stabilization of the intermediate is accomplished by charge/dipole interactions and not by H-bonding as previously suggested. Inclusion of the protein electric field in the calculations does not affect significantly the charge distribution.

**KEY WORDS:** density functional theory calculations; enzyme-intermediate adduct; H-bonding interactions; low-barrier hydrogen bonds; Car-Parrinello simulations

## INTRODUCTION

Hydrogen bonding is one of the most important interactions for the biological function of enzymes. Extensive H-bond networks may stabilize the conformation of the active site which is necessary for the catalytic function and they can fix the optimal orientation of the substrate for the enzymatic reaction. Most importantly, H-bonds may allow for transition state stabilization by lowering the activation free energy by several kcal/mol [2, 3].

A typical example in this respect is constituted by serine proteases (SP's) enzyme family[3, 4, 5, 6, 7, 8, 9, 10, 11, 12, 13].

SP's use the catalytic triad (Ser-195–His-57–Asp-102) to catalyze the hydrolysis of peptides (Fig. 1a). This occurs through nucleophilic addition of the 3-hydroxyl group of Ser-195 to the acyl carbonyl of the substrate, with formation of a negatively charged tetrahedral intermediate (Fig. 1b).

Stabilization of the intermediate is achieved by formation of two H-bond with the amide groups of Ser-195 and Gly-193 (mammalian isoenzymes[4]) or with the amide groups of Ser-195 and the sidechain of Asn-155 (bacterial isoenzymes[14]).

Theoretical[15, 16] and experimental[14, 17] studies on wild type and mutants of a bacterial SP (subtilisin) have shown that Asn-155 is a key residue for the biological function, in that it provides a stabilization of the transition state (TS) relative to the ground state (GS) by as much as  $\approx 5$  kcal/mol. Curiously, no correspondent studies on the mammalian isoenzymes have appeared to shed light on the crucial role of Gly-193[18].

A second, important H-bond interaction involve two residues of the catalytic triad, His-57 and Asp-102. A series of NMR studies on a mammalian[1,

11, 12, 13] and bacterial[20] SP's and their complexes with inhibitors have indicated the presence of a low-barrier hydrogen bond (LBHB) linking  $N_{\delta 1}$  of protonated His-57 with the  $\beta$  carboxyl group of Asp-102 (Fig. 1b)[1, 11, 12, 13]. Approaching of the TS is suggested to facilitate the formation of the LBHB, which in turn may render  $N_{\epsilon 2}$  of His-57 a stronger base for accepting a proton from Ser-195 in the formation of the intermediate[1, 11, 12, 13]. As result of this process, the free energy barrier of TS relative to GS decreases. Ab initio calculations and neutron scattering experiments have led to the conclusion that the LBHB is very covalent in nature[21]. Thus, this "resonance-stabilization" energy could supply much of the energy necessary for enzyme's catalysis[1, 11, 12, 13]. However, the role of this LBHB for the catalytic power of SP's is object of controversy[22, 23].

From the above considerations it is clear that, in spite of its crucial role, the nature and the dynamics of hydrogen bonding in active site of SP are not fully understood. In order to provide a picture of the chemical bonding of these interactions in SP's, and to relate it to the biological function, we have carried out ab initio molecular dynamics simulations [24] on models of SP-intermediate and SP-substrate complexes. This technique is revealing itself as a useful computational tool for investigating specific molecular interactions in biological systems [25]. Based on state-of-the art density functional theory calculations, it describes interactions and charge distributions of (relatively) large systems rather accurately. Furthermore, it includes temperature effects, which obviously play a fundamental role in SP function. Finally, they allow describing bond breaking and bond forming processes at room temperature, which is essential to describe phenomena such as the LBHB.

Anticipating our results, the calculations show that the LBHB is a strongly covalent interaction and that the dramatic Gly-193-induced stabilization of the reaction intermediate is due mainly to the electrostatic interactions between the intermediate and the Asn-192–Gly-193 peptide’s unit dipole.

## COMPUTATIONAL PROCEDURE

### Model complexes.

Our structural models for the adducts of SP with intermediate (I·SP) and substrate (S·SP) are based on the X-ray structure of porcine pancreatic elastase (240 residues) complexed with Ace-Ala-Pro-Val-difluoro-N-phenylethylacetamide (PDB entry: 4EST) [26, 19]. They include the entire catalytic triad, the scissile peptide bond and the oxyanion hole.

The construction of the complexes is carried out in several steps: *i)* the terminal N-phenylethylacetamide is replaced by an acetyl group; *ii)* all hydrogen atoms of the complex, not present in the X-ray structure, are added assuming standard bond lengths and bond angles; *iii)* a shell of 1453 water molecules including the crystallographic ones (approximately corresponding to three water monolayers), is added; *iv)* four chlorine counter ions are added to ensure neutrality; *v)* energy minimization is carried out with the AMBER suite of programs [27] using the AMBER force field [28] (convergence criterion 0.0001 kcal/(mol·Å)). In the minimization, no periodic boundary condition are applied and the electrostatic interactions are calculated assuming a constant dielectric function  $\epsilon = 1$  and without cutoff.

The I·SP and S·SP model complexes comprises the entire side-chain of Asp-102, the imidazole ring of His-57, the Q192G193 peptide linkage and the entire Ser-195 residue, which in I·SP is covalently bound to the substrate (Fig. 2a,b). His-57 is considered doubly protonated in I·SP and protonated in the  $\delta$  position in S·SP [29].

Alternative models representing I·SP and S·SP differ from the previous ones for the substitution of the Q192G193 peptide link with dimethylammonia (Fig. 2c,d).

### Calculations.

The quantum-mechanical problem is solved within the framework of density functional theory (DFT)[30], in its Kohn and Sham (KS)[31] formulation. The KS orbitals are expanded in a plane-wave basis set, up to an energy cut-off of 70 Ry. Only valence electrons are considered explicitly, pseudopotentials of the Martins and Troullier [32] being used for the core-valence electron interaction. BLYP[33, 34] gradient-corrected exchange-correlation functionals are used. The charge of all the complexes is -1.

We have carried out geometry optimization using the direct inversion in iterative subspace (DIIS) method [35, 36] for both electronic (convergence threshold set to  $10^{-5}$ ) and ionic degrees of freedom (convergence threshold set to  $5 \cdot 10^{-4}$ ).

DFT-based Car-Parrinello ab initio molecular dynamics simulations [24] are performed at constant temperature, with the atomic trajectories collected over a period of 0.6 and 1.0 ps for S·SP and I·SP, respectively. Equa-

tions of motion are integrated with the velocity Verlet algorithm. The fictitious electron mass is 400 a.u. and the integration timestep is 4 a.u. Constant temperature simulations are achieved by coupling the systems to a Nosé thermostat[37] at  $T = 300$  K with a frequency of  $500 \text{ cm}^{-1}$ . The terminal hydrogens of Asp-102, His-57, and Gly-193, corresponding to the  $C_\alpha$ ,  $C_\beta$  and  $C_\alpha$  respectively, are kept fixed in their starting position; in S·SP an additional constraint between the  $O_\gamma$ (Ser-195) and the substrate carbon of the scissile bond (indicated in Fig. 2b as  $C_S$ ) is imposed.

Calculations including the external electrostatic potential of the whole protein–water system are also carried out. This potential  $\Phi_{prot}(r)$  at the point  $r$  is evaluated as

$$\Phi_{prot}(r) = \sum_i \frac{q_i}{|r_i - r|} \quad (1)$$

where  $q_i$  are the RESP [38] atomic point charges at point  $r_i$ .

All Car–Parrinello calculations are performed with a parallel version of the CPMD code V3.0h [39].

### Calculated properties.

The electrostatic energy  $\Delta E$  between two moieties (e.g. the intermediate and Q192G193 peptide unit) is calculated as

$$\Delta E = \sum_{ij} \frac{q_i q_j}{r_{ij}}, \quad (2)$$

where the indexes  $i$  and  $j$  refer to atoms of the two moieties.  $q_i$  and  $q_j$  are the partial atomic ESP charges[40] and  $r_{ij}$  is the interatomic distance.

Test calculations are carried out also using the multipolar expansion of the electrostatic energy up to the dipolar term:

$$\Delta E \simeq Q_1\Phi_2 - \boldsymbol{\mu}_1 \cdot \mathbf{E}_2. \quad (3)$$

where  $Q_1$  and  $\boldsymbol{\mu}_1$  are charge and dipole moments of moiety 1 and  $\Phi_2$  and  $\mathbf{E}_2$  the electric potential and the electric field produced by moiety 2. respectively. The results turn out to be very similar to those obtained with eq. 2.

Binding energies (B.E.'s) are calculated as total energies differences between complexes in Fig. 2 and their forming elements. The B.E. of complexes **I** and **III** could not be determined because of the instability of the intermediate fragment.

## RESULTS

In this section, first we analyze structural and electronic features of two models representing the adduct between serine protease and the reaction intermediate (**I** and **III** of Fig. 2). Comparison is then made with features of models of the substrate–enzyme complex (**II** and **IV** of Fig. 2).

### The Intermediate–Enzyme complex

*Structural features and charge distribution.* Conformational properties as well as the H-bond network of the complex are fairly maintained during the dynamics (Fig. 3). Consequently, the charge distribution does not change significantly (with exception of  $C_S$  and  $N_S$ ), as indicated by the ESP atomic partial charges reported for several snapshots of the molecular dy-



namics (Tab. 1). Note that the C<sub>S</sub>-O bond of the intermediate is very polarized towards the oxygen, consistently with the fact that this bond is to be broken in the subsequent step of the hydrolysis. The presence of the protein field does not affect significantly the charge distribution (Tab. 2), suggesting that solvent effects do not play a major role for the electrostatic interaction at the active site.

*H-bond pattern: Asp-102-His-57.* During the dynamics, proton hopping occurs between the His-57 and Asp-102 in the subps time-scale (Fig. 4). The presence of a LBHB is completely consistent with NMR data on an intermediate-serine protease complex, namely the peptidyl trifluoromethyl ketone-chymotrypsin adduct [1].

The chemical bonding of the LBHB can be characterized with the electron localization function (ELF) [41, 42, 43]. The ELF has proven to be very useful to illustrate chemical concepts like localized bonds and electron lone pairs. Fig. 5 shows the ELF before, during and after the proton transfer from His-57 to Asp-102. The red areas indicate strong localization, i.e. spatial regions where the Pauli principle has little influence on the electron distribution.

Fig. 5a shows the presence of the lone pairs of the aspartate oxygen and of the strong electron localization along the histidine N<sub>δ1</sub>-H bond, which indicates the covalent nature of the bond. During the proton transfer (Fig. 5b), the N<sub>δ1</sub>-H bond is still very covalent and an incipient covalent O<sub>δ2</sub>-H bond is being formed. Protonation of Asp-102 establishes a covalent O-H bond: significant portion of ELF is indeed localized on the H atom (Fig. 5c). The formation of the nitrogen electron lone-pair is also evident from the picture. We conclude that the bonding in this LBHB is essentially covalent

in nature. Similar findings have been reported in a very recent ab initio study of low-barrier H-bonds in an organic molecule [21].

*H-bond pattern: Gly-193-intermediate.* The second fundamental H-bond interaction investigated here involves Gly-193 and the intermediate carbonyl oxygen. This H-bond is well maintained during the dynamics (average O $\cdots$ H distance of 1.7(0.1) Å). A rough estimation of the interaction energy based on an electrostatic model (see Computational Section) indicate that Gly-193 stabilizes the intermediate by more than 10 kcal/mol (Tab. 3). This value appears to be too large for a purely electrostatic H-bond interaction [44, 45].

Inspection of the structure reveals that the very large Q192G193 peptide’s unit dipole ( $\approx 4$  D [6]) could be also an important factor for intermediate stabilization, as it points towards the negative charge of the intermediate. To extract the peptide dipolar contribution from the total stabilization energy we construct a second model complex in which the Q192G193 peptide unit is substituted by dimethylammonia (**III** in Fig. 2c). Tab. 3 shows that the resulting stabilization is much smaller, only few kcal/mol. Thus, we conclude that a large contribution of the transition state stabilization is due to electrostatic interaction (charge-dipole interactions).

To study the relevance of the Q192G193 dipole on the dynamics, an ab initio molecular dynamics simulation on complex **III**, where the Q192G193 peptide unit is replaced by a dimethylammonia, is performed. Fig. 6, which reports structural properties of the complex, indicate that this complex is very unstable with respect to the substrate-enzyme complex. Indeed, while the key Gly-193-intermediate H-bond becomes very weak (Fig. 6a), the protonated His-57 transfers a proton to the intermediate (Fig. 6a) and the O $\gamma$  (Ser-

195)–C<sub>S</sub> bond of the intermediate breaks. As a result, a double C<sub>S</sub>–O(I) bond is formed (as indicated by the decrease of the bond distance up to the typical value of a carbonyl peptide bond (1.25 Å in Fig. 6b)) and C<sub>S</sub> changes its hybridization from *sp*<sup>3</sup> to *sp*<sup>2</sup>, with formation of the planar peptide unit (as shown by the increase of the ∠(N(I)–C<sub>S</sub>–O(I)) angle up to ≈ 120° (Fig. 6c)). In conclusion, our calculations suggest that the absence of the stabilizing Q192G193 dipole causes the reverse of the reaction, with formation of the substrate and the original H-bond pattern of the catalytic triad.

### The Substrate–enzyme complex

*Gln-192–substrate interactions.* To estimate the stabilization of the Q192G193 peptide unit’s dipole on the substrate, we perform an ab initio molecular dynamics simulation of a model of the enzyme–substrate adduct (**II** in Fig. 2b).

Fig. 7 shows that during the dynamics the two key H-bond interactions are maintained but no proton transfer occurs. Interestingly, the substrate–protein interaction energy turns out to be much lower than that of the I·SP complex (Tab. 3). Replacing the Q192G19 peptide with dimethylammonia (complex **IV**) causes a drastic decrease of the interaction energy. The latter turns out to be practically identical to that of complex **III** (Tab. 3). We conclude that the H-bond interactions are similar in the S·SP and I·SP complexes. In contrast, the electrostatic (charge–dipole) interactions are very different, the I·SP being more stable by ≈ 6 kcal/mol than S·SP (Tab. 3). It is interesting to note that this value compares well with previous quantum mechanical calculations for the Asn-155–TS stabilization in the bacterial

isoenzyme[15, 16]. We conclude that the transition state stabilization is due mostly to charge–dipole interactions.

For these complexes it has been possible to calculate also the binding energies. Tab. 3 shows a qualitative agreement between binding energies and energies based on electrostatic model. This validates the use of the electrostatic model for a qualitative analysis of intermolecular interactions, as it has been done in this work. However, it must be stressed that use of more realistic quantum mechanical models, which comprises other aminoacids present in the active site cavity, is expected to screen the charges and therefore to reduce the calculated binding energies.

*Charge Distribution.* Also in this complex, most of the ESP charges do not vary significantly during the dynamics and by introducing the electric field of the protein (Tabs. 4 and 5). Most of the ESP charges turn out to be similar to those of the I-SP complex. A notable exception is represented by the C–O peptide bond, which in this case is much less polarized toward the oxygen. Thus it appears that the protein active site, and in particular the Q192G193 moiety, is engineered so as to render the scissile bond more polar in the formation of the transition state.

## DISCUSSION

Within the very short time–scale here explored, our ab initio molecular

dynamics simulations help elucidate important aspects of two key interactions in serine proteases–reaction intermediate complexes, the His-57–Asp-102 LBHB and the Gly-193–intermediate H-bonds.

Our calculations are completely consistent with and confirm the existence of a LBHB between His-57 and Asp-102, which has been observed experimentally in transition state analog inhibitor complexes[1, 11, 12, 13]. Furthermore, they strongly support the proposal of an LBHB–facilitated mechanism[1]. Indeed, the LBHB turns out to be mostly covalent in nature. The energy supplied by covalent interaction may be crucial to overcome the energy loss due to the compression of the two residues, which is a prerequisite of the postulated LBHB–based reaction[1].

The second conclusion of this paper is that the rather large, Gly-193–induced stabilization of the transition state with respect to the fundamental state is not caused by an H-bond with Gly-193, as commonly proposed[4, 5]: indeed, as the H-bond favors the binding of both substrate and intermediate by  $\approx 2.6$  kcal/mol, a value typical of a strong H-bonds in biological systems [45]. Instead, the negatively charged transition state turns out to be more stable relative to S·SP by several kcal/mol as a result of the interaction of the negative charge with the large dipole of the Q192G193 peptide unit. A simulation in which dimethylammonia replaces the Q192G193 peptide unit confirms the crucial role of the dipole: the absence of the stabilizing charge–dipole interaction renders the intermediate species unstable. These considerations suggest that site–directed mutagenesis experiments on the 192 and/or 193 positions might affect significantly the activity of SP’s, as the Q192G193 dipole orientation may be not optimal for transition state stabilization.

Because environment effects may be very important for the chemistry of the active site of this and other enzymes [15, 16, 44, 46], we carry out some of the calculations in the presence of the electric field of the protein. Our results, summarized by tables 1–2 and 4–5, indicate however that the field appears not to affect dramatically the charge distribution of the I·SP and S·SP complexes. More sophisticated models of the protein electric field, which for instance include the electronic polarizabilities of the protein atoms, are not expected to alter significantly the picture.

#### **ACKNOWLEDGMENTS**

Vincent Torre and Frank Alber are gratefully acknowledged for their valuable comments on the manuscript. We acknowledge financial support by Cofinanziamento M. U. R. S. T. (Ministero dell'Università e della Ricerca Scientifica e Tecnologica).

Figure 1: Schematic views of the H-bond network in mammalian serine proteases active site (a) and of the adduct with the intermediate of the enzymatic reaction (b). In (b) the double arrow symbol refers to the a low-barrier H-bond.

Figure 2: Model complexes representing I·SP ((a) and (c)), S·SP ((b) and (d)). In (c) and (d) the Q192G193 peptide unit is replaced by dimethylammonia. H-bonds are depicted with dashed lines. Green arrows indicate the scissile carbon atom  $C_S$ . The latter is labeled only in (b) for clarity.

Figure 3: Molecular dynamics of I·SP: final structure of model **I**. H-bonds are represented with dashed lines.

Figure 4: His-57–Asp-102 H-bond in I·SP (complex **I**):  $H-O_{\delta 2}(\text{Asp-102})$  (red line) and  $H-N_{\delta 1}(\text{His-57})$  (blue line) distances plotted as a function of time.

Figure 5: His-57–Asp-102 proton transfer: electron localization function (ELF) of three snapshot during the dynamics. The ELF is represented in a best-fit plane containing the oxygen, the proton and the imidazole ring, and it ranges from 0 (blue) to 1 (red).

Figure 6: Molecular dynamics of I·SP: selected structural properties of Complex **III** plotted as a function of time. (a) H(Gly-193)–O(I) (blue line), H<sub>ε2</sub>(His-57)–O<sub>γ</sub>(Ser-195) (green line) distances; (b) C<sub>S</sub>–O(I) bond length; (c) N(I)–C<sub>S</sub>–O(I) angle.

Figure 7: H-bonding of S·SP (Complex **II**): H(Gly-193)–O(S) (blue line), O<sub>δ2</sub>(Asp-102)–H<sub>δ1</sub>(His-57) (red line) distances plotted as a function of time.

## References

- [1] Lin J., Westler W. M., Cleland W. W., Markley J. L., Frey P. A. Fractional factors and activation energies for exchange of the low barrier hydrogen bonding proton in peptidyl trifluoromethyl ketone complexes of chymotrypsin. *Proc. Natl. Acad. Sci. USA* 1998; 95:14664-14668.
- [2] Schramm V. L. Enzymatic transition states and transition state analog design. *Ann. Rev. Biochem.* 1998; 67:693-720.
- [3] Fersht A. *Enzyme structure and mechanism*, 2nd ed. New York: W. H. Freeman; 1985. 327 p.
- [4] Kraut J. Serine proteases: structure and mechanism of catalysis. *Ann. Rev. Biochem.* 1977; 46:331-358.
- [5] Stroud R. M. A family of protein-cutting proteins. *Sci. Am.* 1974; 231:74-88.
- [6] Branden C., Tooze J. *Introduction to protein structure*, 2nd ed. New York: Garland; 1999. 410 p.



- [7] Matheson N.R., van Halbeek H., Travis J. Evidence for a tetrahedral intermediate complex during serpin–proteinase interactions. *J. Biol. Chem.* 1991; 266:13489-13491.
- [8] Steitz T. A., Shulman R. G. Crystallographic and NMR studies of the serine proteases. *Annu. Rev. Biochem. Biophys.* 1982; 11:419-444.
- [9] Blow D. M., Birktoft J. J., Hartley B. S. Role of a buried acid group in the mechanism of action of chymotrypsin. *Nature* 1969; 221:337-340.
- [10] Matthews B. W., Sigler P. B., Henderson R, Blow D. M. Three-dimensional structure of tosyl-alpha-chymotrypsin. *Nature* 1967; 214:652-656.
- [11] Lin J., Cassidy C. S., Frey P. A. Correlations of the basicity of His-57 with transition state analogue binding, substrate reactivity, and the strength of the low-barrier hydrogen bond in chymotrypsin. *Biochemistry* 1998; 37:11940-11948.
- [12] Cassidy C. S., Lin J., Frey P. A. A new concept for the mechanism of action of chymotrypsin: the role of the low-barrier hydrogen bond. *Biochemistry* 1997; 36:4576-4584.
- [13] Frey P. A., Whitt S. A., Tobin J. B. A low-barrier hydrogen bond in the catalytic triad of serine proteases. *Science* 1994; 264:1927-1930.
- [14] Bryan P., Pantoliano M. W., Quill S. G., Hsiao H. Y., Poulos T. Site-directed mutagenesis and the role of the oxyanion hole in subtilisin. *Proci. Natl. Acad. Sci. USA* 1986; 83:3743-3745.

- [15] Hwang J. K., Warshel A. Semiquantitative calculation of catalytic free energies in genetically modified enzymes. *Biochemistry* 1987; 26:2669-2573.
- [16] Warshel A., Naray-Szabo G., Sussman F. and Hwang J. K. How do Serine Protease Really Works? *Biochemistry* 1989; 28:3629-3637.
- [17] Wells J. A., Cunningham B. C., Craycar T. P. and Estell D. A. Importance of hydrogen-bond formation in stabilizing the transition state of subtilisin. *Phil. Trans. R. Soc. Lond. A* 1986; 317:415-423.
- [18] The H-bond with Ser-195 is much weaker than that of Gly-193. Indeed, analysis of selected SP-transition state analog complexes (entries 1AI8,1VCG,4EST,1GMH,1SGC,1PO3,7GCH of the Protein Data Bank [19]) shows that  $2.8 \leq d(\text{N}(\text{Ser-195}) \cdots \text{O}) \leq 3.2 \text{ \AA}$  and  $121^\circ \leq \angle(\text{N}(\text{Ser-195})\text{H} \cdots \text{O}) \leq 157^\circ$  and  $2.6 \leq d(\text{N}(\text{Gly-193}) \cdots \text{O}) \leq 2.9 \text{ \AA}$  and  $150^\circ \leq \angle(\text{N}(\text{Gly-193})\text{H} \cdots \text{O}) \leq 160^\circ$  (H atoms obtained assuming standard bond lengths and bond angles).
- [19] Bernstein F. C., Koetzle T. F., Williams G. J. B., et al. The Protein Data Bank: A computer-based archival file for macromolecular structures. *J. Mol. Biol.* 1977; 112:535-542.
- [20] Halkides C. J., Wu Y. Q., Murray C. J. A low-barrier hydrogen bond in subtilisin: <sup>1</sup>H and <sup>15</sup>N NMR studies with peptidyl trifluoromethyl ketones. *Biochemistry* 1996; 35:15941-15948.

- [21] Schiott B., Iversen B. B., Madsen G. K., Larsen F.K., Bruice T. C. On the electronic nature of low-barrier hydrogen bonds in enzymatic reactions. Proc. Natl. Acad. Sci. USA 1998; 95:12799-12802.
- [22] Warshel A., Papazyan A., Kollman P. A. On low-barrier hydrogen bonds and enzyme catalysis. Science 1995; 269:102-106
- [23] Warshel A. Electrostatic origin of the catalytic power of enzymes and the role of preorganized active sites. J. Biol. Chem. 1998; 273:27035-27038.
- [24] Car R., Parrinello M. Unified approach for molecular dynamics and density-functional theory. Phys. Rev. Lett. 1985; 55:2471-2474.
- [25] See, e.g. (a) Roethlisberger U., Carloni P. Ab initio molecular dynamics studies of a synthetic biomimetic model of galactose oxidase. Int. J. Quantum Chem. 1999; 73:209-219. (b) Alber F., Kuonen O., Scapozza L., Folkers G., Carloni P. Density functional studies on herpes simplex virus type 1 thymidine kinase-substrate interactions: the role of Tyr-172 and Met-128 in thymine fixation. PROTEINS: Struct. Func. Gen., 1998; 31:453-459. (c) Molteni C., Parrinello, M. Glucose in aqueous solution by first principles molecular dynamics. J. Am. Chem. Soc. 1998; 120:2168-2171.
- [26] Takahashi L. H., Radhakrishnan R., Rosenfield R. E., Meyer E. F., Trainor D. A. Crystal structure of the covalent complex formed by a peptidyl  $\alpha$ ,  $\alpha$ -difluoro- $\beta$ -keto amide with porcine pancreatic elastase at 1.78 Å resolution. J. Am. Chem. Soc. 1989; 111:3368-3372.

- [27] Case D. A., Pearlman D. A., Caldwell J. W., Cheatham III T. E., Ross W. S., Simmerling C. L., Darden T. A., Merz K. M., Stanton R. V., Cheng A. L., Vincent J. J., Crowley M., Ferguson D. M., Radmer R. J., Seibel G. L., Singh U. C., Weiner P. K., Kollman P. A. AMBER5. University of California, San Francisco; 1997.
- [28] Cornell W. D., Cieplak P., Bayly C. I., Gould I. R., Merz K. M. Jr., Ferguson D. M., Spellmeyer D. C., Fox T., Caldwell J. W., Kollman P. A. A second generation force field for the simulation of proteins, nucleic acids, and organic molecules. *J. Am. Chem. Soc.* 1995; 117:5179-5197.
- [29] Babine R. E., Bender S. L. Molecular recognition of protein–ligand complexes: application to drug design. *Chem. Rev.* 1997; 97:1359-1472 and references therein.
- [30] Hohenberg P., Kohn W. Inhomogeneous electron gas. *Phys. Rev.* 1964; 136:B864-B871.
- [31] Kohn W., Sham L. J. Self-consistent equations including exchange and correlation effects. *Phys. Rev.* 1965; 140:A1133-A1138.
- [32] Troullier N. and Martins J. L. Efficient pseudopotentials for plane-wave calculations. *Phys. Rev. B* 1991; 43:1993-2006.
- [33] Becke A. D. Density-functional exchange-energy approximation with correct asymptotic behaviour. *Phys. Rev. A* 1988; 38:3098-3100.

- [34] Lee C. L., Yang W., and Parr R. G. Development of the Colle–Salvetti correlation–energy formula into a functional of the electron density. *Phys. Rev. B* 1988; 37:785-789.
- [35] Pulay P. Convergence acceleration of iterative sequences. The case of SCF iteration. *Chem. Phys. Lett.* 1980; 73:393-398.
- [36] Hutter J., Lüthi H. P., Parrinello M. Electronic structure optimization in plane–wave–based density functional calculations by direct inversion in the iterative subspace. *Comput. Mater. Sci.* 1994; 2:244-248.
- [37] Nosé S. A unified formulation of the constant temperature molecular dynamics methods. *J. Chem. Phys.* 1981; 81:511-519.
- [38] Cornell W. D., Cieplak P., Bayly C. I., Kollman P. A. Application of RESP charges to calculate conformational energies, hydrogen bond energies and free energies of solvation. *J. Am. Chem. Soc.* 1993; 115:9620-9630.
- [39] Hutter J., Ballone P., Bernasconi M., Focher P., Fois E., Goedecker S., Parrinello M., Tuckerman M. CPMD version 3.0h. MPI für Festkörperforschung and IBM Zurich Research Laboratory, 1995-97.
- [40] Cox S. R. and Williams D. E. Representation of the molecular electrostatic potential by a net atomic charge model. *J. Comput. Chem.* 1982; 2:304-323.
- [41] Becke A. D., Edgecombe K. E. A simple measure of electron localization in atomic and molecular systems. *J. Chem. Phys.* 1990; 92:5397-5403.

- [42] Silvi B., Savin A. Classification of chemical bonds based on topological analysis of electron localization functions. *Nature* 1994; 371:683-686.
- [43] Savin A., Nesper R., Wengert S., Fässler T. F. ELF: The Electron Localization Function. *Angew. Chem. Int. Ed. Engl.* 1997; 36:1808-1832.
- [44] Rao S. N., Singh U. C., Bash P. A. and Kollman P. A. Free energy perturbation calculations on binding and catalysis after mutating Asn-155 in subtilisin. *Nature* 1987; 328:551-554.
- [45] Jeffrey G. A., Saenger W. Hydrogen bonding in biological structures. Berlin: Springer-Verlag; 1991. 591 p.
- [46] Warshel A., Russell S. Theoretical correlation of structure and energetics in the catalytic reaction of trypsin. *J. Am. Chem. Soc.* 1986; 108:6569-6579.

**TABLE 1. I-SP *in vacuo***

Time (ps)	O <sub>γ</sub> (S195)	C <sub>S</sub>	N <sub>S</sub>	O <sub>S</sub>	N (G193)	C (Q192)	O (Q192)	N <sub>δ1</sub> (H57)	N <sub>ε2</sub> (H57)	H <sub>δ1</sub> (H57)	O <sub>δ2</sub> (D102)
Init.	-0.511	1.194	-0.802	-0.717	-0.603	0.504	-0.631	-0.009	-0.072	0.303	-0.907
0.1	-0.509	1.202	-0.529	-0.837	-0.733	0.597	-0.649	-0.084	0.011	0.275	-0.770
0.2	-0.461	1.022	-0.237	-0.724	-0.646	0.571	-0.630	-0.171	0.058	0.286	-0.688
0.3	-0.328	0.835	0.006	-0.658	-0.556	0.516	-0.631	-0.178	0.141	0.298	-0.676
0.4	-0.342	1.083	-0.193	-0.754	-0.582	0.507	-0.625	-0.078	-0.046	0.265	-0.687
0.5	-0.372	1.146	-0.201	-0.794	-0.558	0.505	-0.616	-0.025	-0.150	0.257	-0.665
0.6	-0.407	1.233	-0.480	-0.829	-0.615	0.578	-0.654	-0.042	0.018	0.295	-0.693
0.7	-0.430	1.174	-0.311	-0.883	-0.570	0.563	-0.638	-0.061	0.089	0.284	-0.655
0.8	-0.551	1.245	-0.401	-0.843	-0.487	0.478	-0.620	-0.141	0.001	0.261	-0.601
0.9	-0.504	1.124	-0.202	-0.772	-0.503	0.502	-0.634	-0.127	0.070	0.294	-0.591
1.0	-0.399	1.074	-0.245	-0.827	-0.593	0.636	-0.694	-0.079	0.079	0.294	-0.645
Average	-0.438	1.121	-0.327	-0.785	-0.586	0.542	-0.638	-0.090	0.018	0.283	-0.689
St. Dev.	0.072	0.112	0.207	0.064	0.064	0.048	0.021	0.054	0.079	0.015	0.083

Table 1: Selected ESP partial atomic charges of I-SP *in vacuo*.

**TABLE 2. I-SP with protein external field**

Time (ps)	O $_{\gamma}$ (S195)	C $_S$	N $_S$	O $_S$	N (G193)	C (Q192)	O (Q192)	N $_{\delta 1}$ (H57)	N $_{\epsilon 2}$ (H57)	H $_{\delta 1}$ (H57)	O $_{\delta 2}$ (D102)
0.1	-0.513	1.154	-0.531	-0.876	-0.646	0.640	-0.750	-0.118	0.094	0.354	-0.984
0.2	-0.453	0.931	-0.261	-0.677	-0.527	0.595	-0.722	-0.256	0.122	0.404	-0.914
0.3	-0.329	0.649	-0.037	-0.580	-0.410	0.481	-0.692	-0.273	0.147	0.415	-0.890
0.4	-0.381	0.961	-0.036	-0.739	-0.430	0.400	-0.644	-0.259	0.088	0.374	-0.874
0.5	-0.412	1.000	-0.106	-0.773	-0.358	0.341	-0.611	-0.256	-0.006	0.397	-0.870
0.6	-0.482	1.270	-0.305	-0.929	-0.460	0.447	-0.657	0.015	0.100	0.271	-0.804
0.7	-0.439	1.267	-0.295	-0.932	-0.354	0.504	-0.714	-0.158	0.123	0.336	-0.761
0.8	-0.602	1.373	-0.382	-0.843	-0.349	0.462	-0.720	-0.113	0.031	0.261	-0.669
0.9	-0.606	1.292	-0.221	-0.719	-0.290	0.494	-0.729	-0.117	0.057	0.250	-0.634
1.0	-0.493	1.076	-0.308	-0.802	-0.417	0.596	-0.793	-0.091	0.095	0.396	-0.748
Average	-0.471	1.097	-0.248	-0.787	-0.424	0.496	-0.703	-0.163	0.085	0.346	-0.815
St. Dev.	0.084	0.208	0.148	0.107	0.097	0.088	0.051	0.091	0.044	0.060	0.106

Table 2: Selected ESP atomic charges of I-SP in the presence of the protein electrostatic potential.



**TABLE 3. Intermediate – and substrate – Q192G193 peptide unit interactions**

	ESP	B.E.
$\Delta E$ (I·SP) (Complex <b>I</b> )	-12(4)	—
$\Delta E$ (I·SP) (Complex <b>III</b> )	-2.6	—
$\Delta E$ (S·SP) (Complex <b>II</b> )	-6(2)	-4.2
$\Delta E$ (S·SP) (Complex <b>IV</b> )	-2.6	-1.5

Table 3: Energies (kcal/mol) are calculated from the electrostatic ESP-based model and from binding energies (see Computational Section). ESP-based energies of complexes **I** and **II** are calculated as average during the dynamics, whereas those of complexes **III** and **IV** from the initial structural model.

**TABLE 4. S·SP *in vacuo***

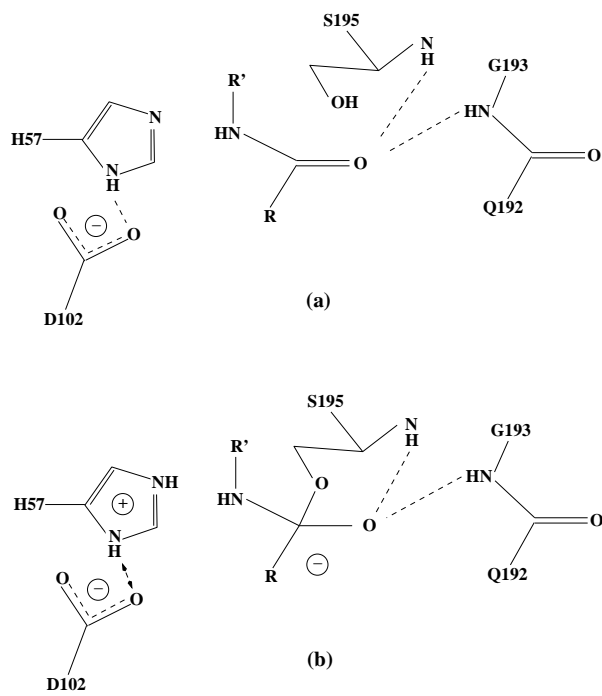
Time (ps)	O <sub>γ</sub> (S195)	C <sub>S</sub>	N <sub>S</sub>	O <sub>S</sub>	N (G193)	C (Q192)	O (Q192)	N <sub>δ1</sub> (H57)	N <sub>ε2</sub> (H57)	H <sub>δ1</sub> (H57)	O <sub>δ2</sub> (D102)
Init.	-0.468	0.635	-0.352	-0.469	-0.561	0.585	-0.637	0.044	-0.237	0.258	-0.869
0.1	-0.473	0.739	-0.527	-0.559	-0.709	0.624	-0.644	0.135	-0.237	0.206	-0.785
0.2	-0.410	0.578	-0.259	-0.574	-0.595	0.599	-0.635	-0.072	-0.219	0.313	-0.869
0.3	-0.528	0.684	-0.280	-0.595	-0.638	0.605	-0.640	-0.068	-0.458	0.317	-0.879
0.4	-0.476	0.585	-0.219	-0.519	-0.642	0.633	-0.643	-0.156	-0.472	0.374	-0.875
0.5	-0.491	0.618	-0.165	-0.577	-0.592	0.630	-0.658	0.070	-0.476	0.254	-0.835
0.6	-0.355	0.576	-0.189	-0.549	-0.628	0.616	-0.644	0.149	-0.231	0.233	-0.824
Average	-0.457	0.631	-0.284	-0.549	-0.624	0.613	-0.643	0.015	-0.333	0.279	-0.848
St. Dev.	0.053	0.057	0.114	0.040	0.044	0.016	0.007	0.107	0.118	0.054	0.032

Table 4: Selected ESP atomic charges of S·SP *in vacuo*.

**TABLE 5. S·SP with protein external field**

Time (ps)	$O_\gamma(\text{S195})$	$C_S$	$N_S$	$O_S$	N (G193)	C (Q192)	O (Q192)	$N_{\delta 1}(\text{H57})$	$N_{\epsilon 2}(\text{H57})$	$H_{\delta 1}(\text{H57})$	$O_{\delta 2}(\text{D102})$
Init.	-0.331	0.693	-0.474	-0.488	-0.614	0.686	-0.645	-0.004	-0.124	0.287	-0.912
0.1	-0.418	0.703	-0.602	-0.552	-0.701	0.745	-0.782	-0.199	-0.256	0.345	-0.803
0.2	-0.349	0.492	-0.389	-0.513	-0.574	0.722	-0.768	-0.217	-0.315	0.334	-0.840
0.3	-0.477	0.601	-0.356	-0.546	-0.667	0.825	-0.789	-0.104	-0.553	0.296	-0.860
0.4	-0.475	0.561	-0.301	-0.495	-0.650	0.812	-0.765	-0.186	-0.576	0.343	-0.843
0.5	-0.455	0.553	-0.262	-0.524	-0.570	0.772	-0.787	-0.129	-0.612	0.296	-0.827
0.6	-0.341	0.496	-0.273	-0.497	-0.650	0.775	-0.769	-0.172	-0.306	0.348	-0.835
Average	-0.407	0.586	-0.380	-0.516	-0.632	0.762	-0.758	-0.144	-0.392	0.321	-0.846
St. Dev.	0.060	0.079	0.114	0.023	0.045	0.045	0.047	0.068	0.174	0.025	0.025

Table 5: Selected ESP atomic charges of S·SP in the presence of the protein electrostatic potential.



**Fig. 1. De Santis L., Carloni P.**

This figure "Fig2.gif" is available in "gif" format from:

<http://arxiv.org/ps/physics/9907003v1>

This figure "Fig3.gif" is available in "gif" format from:

<http://arxiv.org/ps/physics/9907003v1>

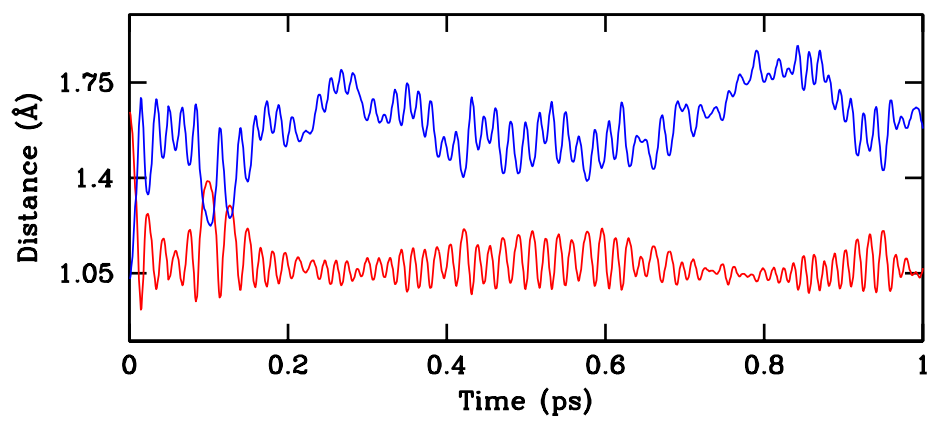


**Fig. 4. De Santis L., Carloni P.**

This figure "Fig5.gif" is available in "gif" format from:

<http://arxiv.org/ps/physics/9907003v1>



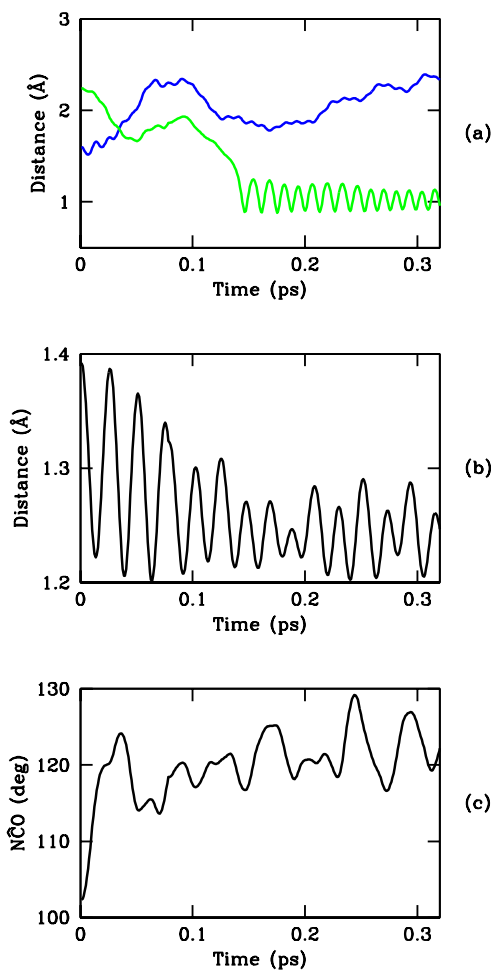


**Fig. 6. De Santis L., Carloni P.**

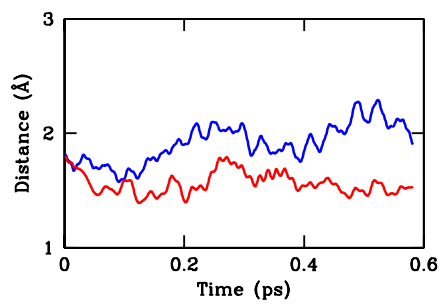


**Fig. 7. De Santis L., Carloni P.**